Structure-Activity Relationships in Purine-Based Inhibitor Binding to HSP90 Isoforms

Lisa Wright,[1] Xavier Barril,[1] Brian Dymock,[1]
Louisa Sheridan,[1] Allan Surgenor,[1]
Mandy Beswick,[1] Martin Drysdale,[1] Adam Collier,[1]
Andy Massey,[1] Nick Davies,[1] Alex Fink,[1]
Christophe Fromont,[1] Wynne Aherne,[2]
Kathy Boxall,[2] Swee Sharp,[2] Paul Workman,[2]
and Roderick E. Hubbard[1],*
[1]Vernalis (R&D) Ltd.
Granta Park
Abington, Cambridge CB1 6GB
[2]Cancer Research UK Centre for
    Cancer Therapeutics
Institute of Cancer Research
Sutton, Surrey
United Kingdom

Summary

Inhibition of the ATPase activity of the chaperone protein HSP90 is a potential strategy for treatment of cancers. We have determined structures of the HSP90α N-terminal domain complexed with the purine-based inhibitor, PU3, and analogs with enhanced potency both in enzyme and cell-based assays. The compounds induce upregulation of HSP70 and downregulation of the known HSP90 client proteins Raf-1, CDK4, and ErbB2, confirming that the molecules inhibit cell growth by a mechanism dependent on HSP90 inhibition. We have also determined the first structure of the N-terminal domain of HSP90β, complexed with PU3. The structures allow a detailed rationale to be developed for the observed affinity of the PU3 class of compounds for HSP90 and also provide a structural framework for design of compounds with improved binding affinity and drug-like properties.

Introduction

HSP90α, HSP90β, GRP94, and TRAP-1 are members of a highly abundant family of human chaperones responsible for the maturation and activity of a variety of key client proteins involved in cell growth and proliferation (see [1], [2], and references therein).

HSP90 function is ATP dependent and an intrinsic ATPase activity is required for the operation of a functional "chaperone" cycle, which leads to the stabilization of client proteins [3]. It is thought that all of the HSP90 family members have a similar mode of action but act on different client proteins dependent, in part, on their localization within the cell [1].

The HSP90 proteins have three domains. The C-terminal domain is the site for homodimerization of the proteins and contains binding sites for cochaperones. This domain has recently been shown to be important for autophosphorylation of the protein and may also

*Correspondence: r.hubbard@vernalis.com

contain a binding site for novobiocin [4, 5]. The structure of the middle domain for the yeast homolog of HSP90 has been determined recently [6]. This displays a large hydrophobic surface, implicated in stabilizing the fold of client proteins. The N-terminal domain (hereafter Nt-HSP90) is the most studied and contains an unusually shaped ATP binding cleft, known as the Bergerat fold, responsible for the ATPase activity important for function [7].

Previously, structures of human Nt-HSP90α and yeast Nt-HSP90 have been published both in the unliganded form (apo-) and in complex with a variety of inhibitors (summarized in [3] and [8]). The protein has the α/β fold of the GHKL superfamily [9] with a 7-stranded β sheet forming the main core of the protein with 4 α helices forming the compact cavity that binds ATP. The overall structure of the proteins from yeast and human are very similar.

The N-terminal domain of HSP90 provides all of the structural requirements for nucleotide binding. However, it alone has relatively little ATPase activity, and contacts from the middle domain of full-length HSP90 are also required to ensure functionality of the enzyme. The catalytic residues Arg 380 and Gln 384 are contributed by the middle segment of HSP90, and both in vitro and in vivo studies have confirmed their essential involvement in ATPase activity and chaperone function. The "catalytic loop" bearing Arg 380 and Gln 384 shows significant flexibility, varying between a helical structure where these residues are directed out of the ATP binding site to an extended loop in which they could reach into the ATP binding site and interact with bound ATP [6].

The HSP90 ATPase activity can be selectively inhibited by natural product antibiotics such as geldanamycin or radicicol [1]. Recent studies with geldanamycin derivatives suggest that cancer cells are particularly sensitive to HSP90 inhibition, inducing cell cycle arrest and apoptosis. Although the exact mechanism for the tumor cell selectivity of these natural products has yet to be fully elucidated, the most compelling suggestion is a tumor cell dependence on key signaling proteins that are clients of the HSP90 family of chaperones. Exposure to HSP90 inhibitors results in depletion of a number of oncogenic client proteins, including Raf-1, ErbB2, Akt/PKB, CDK4, Met, POLO-1, mutant p53, and the androgen/estrogen receptors. A particular therapeutic advantage of HSP90 inhibitors may result from their simultaneous combinatorial effects on multiple oncogenic proteins and pathways that are responsible for driving malignant progression [1, 2]. The radicicol and geldanamycin natural product classes of HSP90 inhibitors have significant limitations, for example, with respect to ADME properties [1]. The development of improved, synthetic inhibitors is therefore an important objective.

Chiosis et al. have described the design of a series of purine analogs (the lead molecule being PU3, compound 1) and measured binding affinity and cellular activity [10, 11]. We have recently published an initial report on the design of PU3 analogs with enhanced activity in
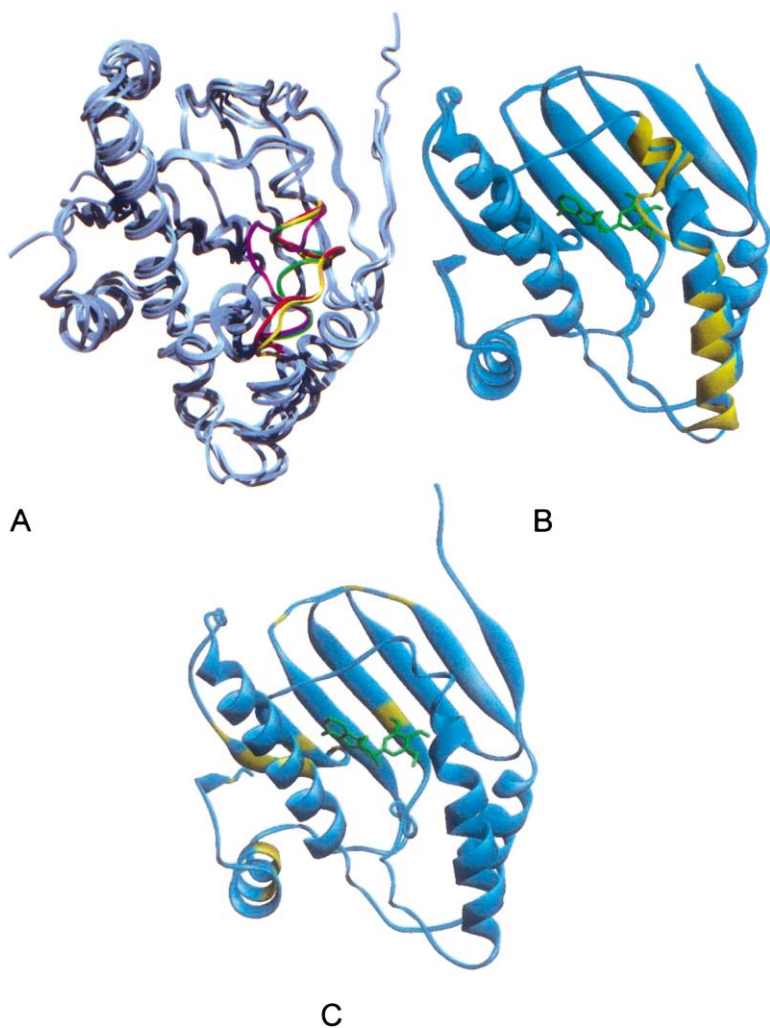
Figure 1. Structures of Nt-HSP90 Isoforms

(A) Comparison of the structure of some apo-Nt-HSP90 proteins. The proteins are overlaid on all main chain atoms except for residues 104–111, which are colored in yellow for the tetragonal form of yeast HSP90 (PDB ID code 1AH6), red for orthorhombic form of yeast HSP90 (1AH8), green for human HSP90α (1YES), and purple for the apo-Nt-HSP90α structure reported here. This figure (and Figures 4 and 6) was produced using QUANTA (Accelrys, San Diego).

(B) Comparison of apo (yellow) and PU3 bound (light blue) Nt-HSP90α highlighting the secondary structure (wider ribbons) and PU3 (in green stick). This figure (and [C] and Figure 3) was produced using ViewerPro (Accelrys, San Diego).

(C) The structure of human Nt-HSP90β with PU3 bound (green stick). Amino acid differences between HSP90α and HSP90β are shown in yellow.

both enzyme and cell-based assays [12]. Here, we report the structures of Nt-HSP90α complexed to a series of PU3 analogs and demonstrate how a detailed analysis of the structures provides a rationale of the observed changes in activity of these and the previously reported PU3 analogs. In addition, we report the first determination of the structure of the homologous Nt-HSP90β bound to the inhibitor PU3.

Results and Discussion

### Structure of Apo-Nt-Human HSP90α

We have independently determined and refined the structure of human apo-Nt-HSP90α at 1.42 Å resolution in the presence and absence of an N-terminal hexahistidine tag. The structures are essentially identical to the "closed" conformation for the protein described by Stebbins et al. ([8]; Protein Data Bank [PDB] ID code 1YER), and no density can be observed for the tag. Figure 1A shows a comparison of our structure with other published apo forms of human Nt-HSP90α and yeast Nt-HSP90. The main variation between structures is in the conformation of residues 104 to 111. In some yeast structures, this region adopts a helical conforma-

tion, whereas, in other yeast and some human structures, this helix unwinds to form an "open" conformation. In the Nt-HSP90α structure reported here, this region unwinds to form a loop that extends over the binding site, effectively closing it. These comparisons demonstrate that there is considerable plasticity in this region of the structure, which is at the entrance to the ATP binding site. Some of the residues seen as important for binding to ligands are in this loop, e.g., Leu 107.

Structure of Nt-HSP90α in Complex with PU3

Figure 1B compares the structure of Nt-HSP90α determined from crystals grown in the presence and absence of the compound PU3, and Figure 2 shows a schematic representation of the interactions made between PU3 and the protein binding site. The ligand sits in the ADP binding site with essentially no change in conformation across most of the protein structure. However, the region 104–111 adopts a helical conformation, providing space for binding of the trimethoxy phenyl moiety of PU3. This change in conformation of the helix introduces a channel through the protein running from the ATP binding site behind the helix and out to solvent. It is mainly hydrophobic in nature, although three water mol-
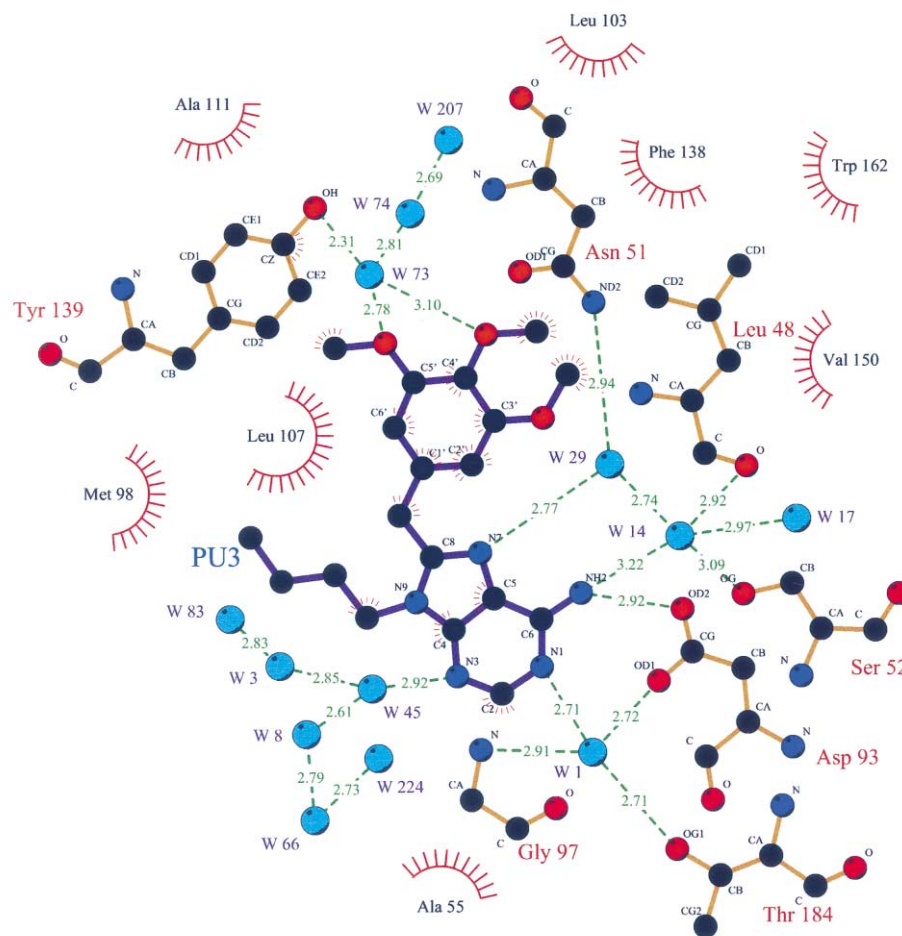
Figure 2. PU3 Binding to HSP90

Schematic of interactions between PU3 and the binding site of Nt-HSP90α (figure produced using Ligplot, [32]).

ecules do sit in the channel, making hydrogen bonds with one of the methoxy groups of the PU3 ligand and with various residues within the channel.

Human Nt-HSP90β in Complex with PU3

Figure 1C shows the structure of Nt-HSP90β with PU3 bound. The overall structures of α and β are essentially identical (rmsd 0.39 Å when overlapped on all main chain atoms), and the same changes are seen in the conformation of loop 104–111. The majority of residues that differ in sequence between the two isoforms are located within the β sheet on the opposite side of the molecule from the binding site (highlighted in yellow). Only one residue (Val144) is close to the ligand, but the side chain is facing away from the binding site. In our hands, production and crystallization of Nt-HSP90α is more rapid

and reproducible than for Nt-HSP90β, so all subsequent work has been conducted with the α isoform.

Comparison of Ligand Binding

Figure 3 shows the detail of the binding sites of Nt-HSP90α with PU3, ADP [13], geldanamycin [8], and radicicol [14] bound. The key interactions with Asp 93 are preserved in all complexes, with a network of hydrogen bonds around the carboxylate of Asp93 involving Asn51, Ser52, Thr284, Gly97, and four water molecules consistently found in the same positions. Three of these waters are hydrogen bonded to ADP, PU3, and geldanamycin, while radicicol interacts with two waters and displaces a third one. The important role played by the crystallographic waters in the recognition of the ligands by HSP90 is further supported by the almost identical local-
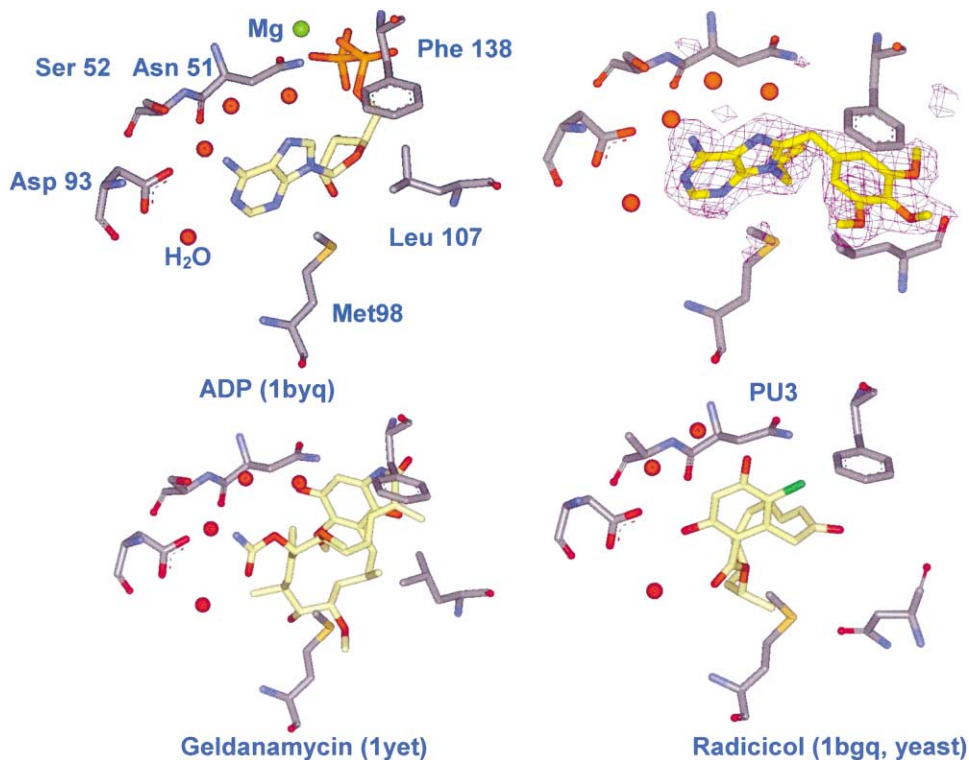
Figure 3. Binding of Ligands to Nt-HSP90α

Key protein residues and water molecules shown for ADP (from PDB ID code 1BYQ, human), PU3 (this paper), geldanamycin (1YET, human), and radicicol (1BGQ, yeast). In addition, the PU3 panel includes an Fo-Fc electron density map contoured at 2.8 σ, calculated for the final refined structure with PU3 omitted. Carbon atoms for the protein are in dark gray and for ligand in light yellow. Oxygen atoms are red, nitrogen blue, sulfur yellow, and phosphorus orange. Water molecules are shown as small red spheres. Note that the equivalent residue to Leu 107 in human HSP90 is Asn in yeast.

ization of these water molecules across all the structures available so far.

Most of the van der Waals contacts established between the ligands and the residues defining the cavity around Asp93, namely Asn51, Ser52 (Ala38 in yeast), Ala55, Met98, and Thr184, are also conserved, but further away from Asp93 the interactions are less conserved. For instance, the Mg^{2+} ion seen in ADP-bound structures is not required for the binding of other ligands, and polar interactions with groups such as Nζ of Lys58, Nζ of Lys112, and N of Phe138 are ligand specific.

The PU3 Binding Mode

PU3 was designed with a purine ring to mimic the adenine of ADP/ATP and a trimethoxy phenyl ring to reach toward the phosphate binding region of the ATP binding site [10]. From our structures, it can be seen that the purine ring of PU3 does bind in the same position as that of ADP (rmsd ≈ 0.5 Å). However, the formation of a helix by residues 104–111 creates a channel that accommodates the trimethoxy phenyl ring of the ligand. Chiosis et al. used the "open" structure of HSP90 (PDB ID code 1YET) to manually dock PU3 in the ATP binding site, and protein flexibility was only considered by minimization of the resulting complex [10]. Our structures show that PU3 induces a conformational change that transforms the shape of the phosphate binding region

of HSP90, and so it is not surprising that the previously predicted binding mode was incorrect. The new channel has striking chemical complementarities for the ligand, as seen in Figure 2. The aromatic ring of PU3 is stacked between the side chains of Phe138 and Leu107 and forms other favorable hydrophobic interactions with Met98 (Sδ) and Leu103 (Cδ2). In addition, the methyls of the methoxy groups make favorable hydrophobic contacts with the aromatic rings of Trp162 and Tyr139 as well as with the aliphatic carbons of Ala111 and Val150. The only residues in the binding site that change conformation are those in the flexible helix, while Phe138, Met98, Val150, Trp162, and Tyr139 remain in the same conformation. The end of the channel is more hydrophilic, lined with polar atoms from Leu103 (O), Trp162 (Nϵ), Tyr139 (Oη), and Gly108 (N). These maintain a network of water molecules that can interact with the oxygen atoms of the methoxy groups in R4 and R5.

The alkyl chain at N9 of PU3 is located in the same position as the ribose of ADP, but the exit from the binding pocket has a different shape in the two complexes. In particular, Leu107 is displaced by approximately 4 Å, blocking the space in the direction of the N9-R' bond in the PU3 complex. At either side of Leu107, Met98 and the phenyl ring of PU3 are also limiting the space available for N9 substituents. As a result, this position is more impeded for PU3 than for ADP binding.
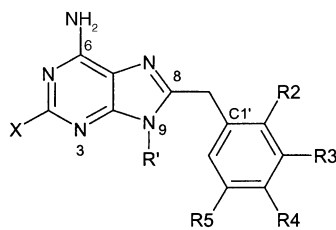
Compds	X	R²	R³	R⁴	R⁵	R'	IC₅₀ ATPase (μM)§	PDB Code	Resolution
1 (PU3)	H	H	OMe	OMe	OMe	n-butyl	>200	1uy6	1.9
2	H	H	H	OMe	H	n-butyl	>200	1uy7	1.9
3	H	H	OMe	H	H	n-butyl	75+/-13	1uy8	2.0
4	H	H	OCH₂O Bridge		H	n-butyl	15.3+/-2	1uy9	2.0
5	H	OMe	H	H	OMe	n-butyl	41+/-9	1uyc	2.0
6	H	Cl	OMe	OMe	OMe	n-butyl	>200	1uyd	2.2
7	H	Cl	OMe	OMe	OMe	1-pentynyl	>200	1uye	2.0
8	F	Cl	OMe	OMe	OMe	1-pentynyl	30+/-8	1uyf	2.0
9	F	OMe	H	H	OMe	H	53.5+/-4	1uyg	1.95
10	F	OMe	H	H	OMe	n-butyl	14.3+/-5	1uyh	2.2
11	F	OMe	H	H	OMe	1-pentynyl	4.1+/-0.1	1uyi	2.2
12	F	H	OCH₂O Bridge		H	n-butyl	17.1+/-9	1uyk	2.6
17AAG							13.4+/-3		
Radicicol							<0.2		

§ all IC₅₀ values are the average of at least 2 determinations
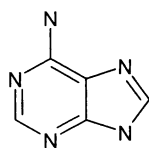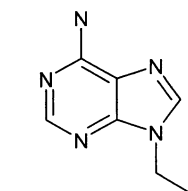

Adenine   9-ethyl adenine

Figure 4. Purine Analogs and Enzyme Inhibition Data

Both the amino acid composition and the shape of the Bergerat fold are well conserved within the GHKL superfamily [9]. This structural similarity allows cross-reactivity, as shown by the strong inhibition of branched-chain α-keto acid dehydrogenase kinase by radicicol [15]. The residues that line the new channel do not show any significant sequence or structural homology with other members of the GHKL superfamily (data not shown), suggesting a route to specific HSP90 inhibitors.

Activity of PU3 Analogs

We have synthesized a series of PU3 analogs (Figure 4) and determined the structures of the complex between each of the compounds and Nt-HSP90α. 1 is the original

PU3 and 8 the most active published PU3 analog [11], where the affinity of PU3 for HSP90 was measured by an immobilised geldanamycin displacement assay (a binding assay). In our study, the activity of the compounds has been measured as IC₅₀ for inhibition of the ATPase activity of full-length yeast HSP90α based on a malachite green assay [16]. For comparison, PU3 (1) is not active in the ATPase assay (>200 μM), whereas it is 15–20 μM in the binding assay. The most potent compound of Chiosis et al. (8) is 30 μM in the ATPase assay, and it was reported as 0.55 μM in the binding assay.

The cellular activity of compounds 1, 8, and 11 was measured using a growth inhibition (GI) assay on the

Compound 1 (PU3)

Compound 8
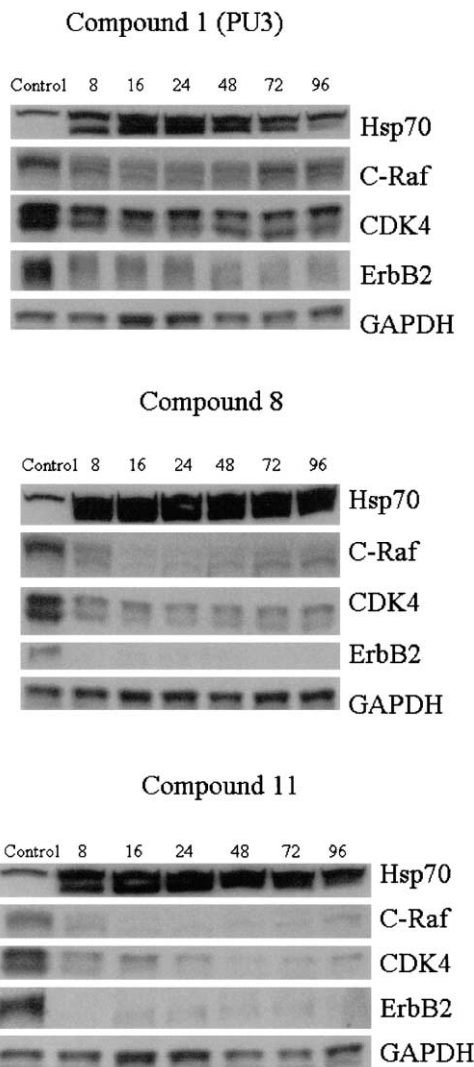
Compound 11

Figure 5. PU3 Ligands Elicit HSP90 Molecular Signature

HCT116 cells were exposed to compounds 1, 8, and 11 at concentrations of 100 μM for 1 (2×GI50) and 17 μM for 8 and 16.5 μM for 11 (5×GI50) as described in the main text. Cell lysates obtained after 8, 16, 24, 48, 72, or 96 hr incubation were subjected to Western blot determination of HSP70, Raf-1, CDK4, and ErbB2. 17AAG is included as a positive compound control, and protein loading was established by GAPDH determination.

human colon tumor cell line, HCT116, giving GI$_{50}$ values of 50 μM, 3.4 μM, and 3.3 μM, respectively. This compares well with the GI$_{50}$ of 2 μM reported by Chiosis et al. for 8 (compound 71 in [11]). Additional experiments were also performed to measure the pattern of expression of proteins that are known to be affected by specific HSP90 inhibition [17]. Western blot assays were used to measure the upregulation of the chaperone HSP70 and downregulation of the HSP90 client proteins Raf-1, CDK4, and ErbB2. This was measured at either twice (for compound 1 because of solubility limitations) or five times (for compounds 8 and 11) the GI$_{50}$ required for cell growth inhibition. Figure 5 shows a series of Western blots showing the levels of different proteins present in cells following exposure of compound to HCT116 cells.

For all compounds, the inhibitors induce upregulation of HSP70, which is depleted over time. Although there is some variability, compounds consistently induce downregulation of CDK4 ErbB2, and Raf-1.These results indicate that cell growth inhibition is occurring by a mechanism dependent on HSP90 inhibition.

Structure-Activity Relationships of PU3 Analogs
A variety of molecular modeling calculations and analyses can use the structures of the compounds bound to the protein to rationalize the observed structure-activity relationships (SAR) for not only the compounds in Figure 4, but also the activity reported for previously published compounds by Chiosis et al. [10, 11].

Effect of Different Methoxy Substitution on the Phenyl Ring
We analyzed the effect of different patterns of methoxy group substitution on the trimethoxy phenyl ring group of PU3. As expected for a region where ligand and protein are closely packed, the behavior that we have observed is not additive. The measured activity is always a result of the balance between different forces (internal energy, hydrophobic interactions, polar interactions, induced effects, shape complementarity, etc.) and, given the complexity of the system, is often difficult to understand without a careful analysis of the structure.

A compound with a single methoxy group at R3 is more potent than the original trimethoxy compound (3, IC$_{50}$ = 76 μM versus 1, IC$_{50}$ > 200 μM). This is somewhat surprising, as the oxygen is not making any polar interaction and is buried in a hydrophobic cavity created by Met98 and Val150. Even more intriguingly, the R4 single methoxy compound is inactive (2, IC$_{50}$ > 200 μM), even though the oxygen is interacting with a network of water-mediated hydrogen bonds involving Oζ of Tyr139, Nϵ1 of Trp162, and O of Leu103. Close inspection of the structures of these compounds bound to Nt-HSP90α shows that the binding of 2 is penalized by the presence of a void in the cavity, whereas 3 provides much better shape complementarity and packing between receptor and ligand.

Figure 6A shows an overlay of the structures of 3 and 2 together with the structures of PU3 and the 2,3-methylenedioxy compound, 4. This emphasizes that the methyl groups of 3 and 2 are found in approximately the same position, making a close contact with the aromatic system of Trp162. 4 combines both methoxy features in a five-membered ring. This compound combines the good packing features of 3 with the water-mediated hydrogen bonding of 2, making it one of the most active compounds within our PU3 series (IC$_{50}$ = 14 μM).

This analysis suggests that methoxy groups at both positions R3 and R4 would be difficult to accommodate. A comparison of the whole series of compounds (Figure 6B) emphasizes that the trimethoxy compounds adopt a slightly different conformation, with the methyl group of the R4 methoxy pushed toward the hydrophilic environment of the solvent channel, while the oxygen of the R4 methoxy remains in the hydrophobic cavity. Thus, although the methoxy at R2 provides a set of water-mediated interactions, the other methoxy groups are in unfavorable positions, giving rise to the relatively poor activity seen for PU3.

A
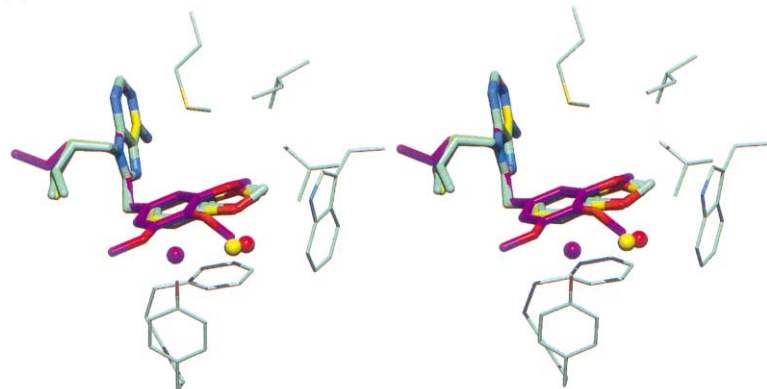
B
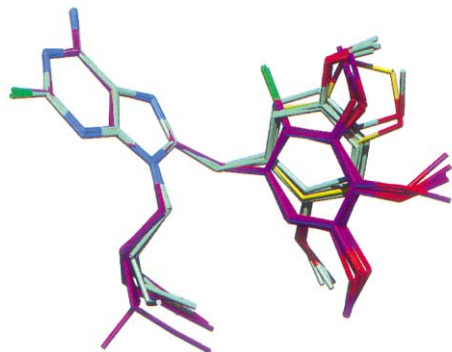
Figure 6. Comparison of PU3 Ligands

(A) Stereo figure showing the structure of four compounds overlaid together with selected amino acids (Trp 162, Met 98, Leu 107, Val 150, Phe 138, and Tyr 139) for a representative protein structure (with compound **2** bound). Nitrogens are blue, oxygens are red, and sulphurs are yellow. For the protein, carbons are green, with the carbons of different compounds colored as follows: purple is **1**, yellow is **4**, and green are **2** and **3**. A key water molecule is shown as a sphere, absent in the **3** structure.

(B) The structure of the 12 featured PU3 analogs bound to Nt-HSP90α, overlaid on the purine ring. Nitrogens are blue, oxygens are red, and fluorine or chlorine are light green. The carbons of the trimethoxy benzene-containing compounds (**1**, **6**, **7**, and **8**) are in purple, the carbons of the OCH$_2$O bridged compounds (**4** and **12**) are yellow, and the carbons of the other compounds are pale green.

One outcome of this analysis was the design and synthesis of **5**, which has methoxy groups at R2 and R5. The addition of a methoxy group at R2 roughly doubles the potency (cf. IC$_{50}$ 41 μM versus IC$_{50}$ for **3** of 75 μM), which can be explained by the formation of an additional water-mediated hydrogen bond between the methoxy group and N of Phe138.

Effect of Substitutions at R2

Substitutions at R2 were investigated by Chiosis et al. [11] with chlorine and bromine. Cl provides improved activity, mono-Br is approximately as active as PU3, and di-Br is completely inactive. The structures of **7** and **8** show that the atom of chlorine participates in many hydrophobic contacts with the side chains of Met98, Phe138, Val150, and Val186. The packing of this atom is extremely compact, particularly with Phe138 and Met98, with the closest contacts being almost exactly the sum of the van der Waals radii. These are very favorable dispersion and hydrophobic interactions, with the calculated van der Waals term alone accounting for 2 kcal/mol [18]. Both the bond distance and the van der Waals radii of bromine are larger than that of chlorine, suggesting that the mono-bromine could only be accommodated by changes in conformation of the phenyl ring and/or adjustments in the pocket, while the di-bromo compound will not fit.

The increase in potency from the favorable interaction of Cl is essentially cancelled out by internal strain in the ligand from steric clashes between Cl and the purine ring. Quantum-mechanical (QM) calculations at B3LYP/6-31G(d) level of theory indicate that the conformation observed in the crystal is 2.7 kcal/mol less stable in vacuo than the conformation in which a rotation of 180° has been performed along the axis of the C10-C1′ bond.

Choice of Linker between Purine and Methoxy Phenyl Group

Chiosis et al. [11] found that only –CH$_2$– was suitable as a linker between the purine and trimethoxy phenyl ring systems to give active compounds. The relative orientation and position of the purine binding site (Bergerat fold) and the channel have tight constraints. Larger groups (such as –O–CH$_2$–) will result in a misplacement of the phenyl ring, while groups that could be conjugated, such as N, will drive the rings toward a coplanar orientation, therefore penalizing the perpendicular conformation required to fit the binding site. Figure 6B emphasizes the variation seen in the methoxy series of structures, where the angle at the methylene bridge ranges from 110 (para-monomethoxy **2**) to 120 (1-pentyne trimethoxybenzyl **8**). This conformational preference has been analyzed through QM calculations at B3LYP/6-31G(d) level of theory. These show that the angle of minimum energy is 115.5°, and that all angles between 110° and 120° are within 0.5 kcal/mol of this minimum. The QM calculations also indicate that the observed dihedral angles ϕ1 (N9-C8-CH2-C1′, which

ranges from $-58°$ to $-81°$) and $\phi2$ (C8-CH2-C1'-C2', which ranges from $-24°$ to $-56°$) are preferred over planar ($\phi1 = 180$) or V-shaped conformations ($\phi2 = 90$). When the methylene bridge is replaced by oxygen, the angle of minimum energy becomes $120.6°$, and smaller torsions are heavily penalized ($\alpha = 110$; $\Delta H = 2.2$ kcal/mol). In addition, the planar conformation is preferred over the perpendicular ($\phi1 \approx 180$; $\phi2 \approx 0$; $\Delta H = -2.5$ kcal/mol). This, we believe, explains why such substitution produces inactive compounds [11].

Substitution at C2

The purine ring of PU3 fits tightly into the ATP binding pocket of the protein. It is therefore not surprising that there is little scope for substitution of bulky or rigid groups such as iodine, cyano, or vinyl at C2, primarily because of the steric hindrance from the backbone of Gly 97. However, fluorine at position C2 does provide compounds with increased potency. We have used molecular interaction potential calculations (MIP) [19] to obtain an explanation for this effect, using 8,9-dimethyl-adenine and 8,9-dimethyl,2-fluoro-adenine as models of PU3 analogs (results not shown). The comparison of the potential shows that the fluorine atom polarizes the molecule and increases the interaction potential of N1 and the exocyclic amine, enhancing the interaction with Asp93 and the crystallographic waters. In addition, the negative charge density over the fluorine also increases the dipole and contributes to the improved solubility reported by Chiosis et al. [11].

Alkyl Side Chain at N9

The structure of PU3-bound HSP90 shows that the first and second methylenes of the alkyl chain interact with residues Leu107 and Met98 of HSP90, forming favorable hydrophobic interactions. These molecular contacts are important for binding, as shown by the poor inhibitory activity of N9-unsubstituted compounds. The remainder of the side chain is solvent exposed and does not appear to make contact with the protein. As described above, the N9 position is sterically hindered, which means that groups too bulky or not flexible enough to be accommodated in this restricted space will result in steric clashes with the protein and/or the phenyl ring of PU3. In either case, the consequence would be decreased activity. This explains why all the 9-N-alkylated compounds derived from secondary alcohols are inactive (compounds 29, 30, 31, 33, and 34 [11]), as are most of the compounds substituted at the second carbon (compounds 28, 39, 40, 43, 44, and 45 [11]). The only exception is compound 16, which benefits from small substitutents (cyclopropyl and methyl).

After the first two carbons, the cavity opens to bulk solvent, allowing a wider range of groups. This explains the relatively flat SAR observed in this area, and, as can be seen in Figure 6B, there is some flexibility in the conformation of the alkyl chain. Nevertheless, some compounds (particularly pentyne) are significantly more active than others, perhaps due to the ability of the alkyne group to provide some hydrogen bonding capacity. In the structures of 7 and 8, the alkyne group makes an interaction with the carbonyl oxygen of Gly 135, whereas a change in the conformation of the alkyl chain leaves the alkyne group pointing toward the acidic side chain of Asp 102 in 11.

Binding of Purine Fragments

We have determined the structures of Nt-HSP90α crystals soaked with 22 mM adenine and with N9-ethyl adenine (data not shown). These structures show that the fragments bind in the same position as seen for the purine moieties of PU3 and ADP. In addition, the binding of these fragments to protein was monitored through saturation transfer difference measurements using NMR spectroscopy (see Experimental Procedures). No binding could be observed for 1 mM adenine binding to 10 μM Nt-HSP90α protein. However, binding could be seen for N9-ethyl adenine, and this binding was displaced by addition of 100 μM PU3. It is difficult to determine the affinity of fragments seen in such NMR or X-ray experiments, as binding is influenced by many kinetic effects (such as exchange kinetics or crystal lattice). However, the results suggest that N9-ethyl adenine is binding with an affinity greater than 5–10 mM and that adenine is binding with weaker affinity. This level of affinity is consistent with the lack of activity seen for the Ad-But compound from Chiosis et al. [10]. These observations also emphasize that although the core purine fragment binds to the active site, much of the affinity of binding to HSP90 by the PU3 analogs comes from other portions of the compounds.

Binding of Biotinylated PU3

The results presented above provide a satisfying rationale for the observed structure-activity relationships for the PU3 series of compounds. The binding of the ligand to the protein locates the purine moiety in the expected position, and the trimethoxyphenyl portion of the ligand exploits the creation of a new pocket formed from a region of the protein that is seen to be conformationally flexible across a number of crystal structures. The relative position and orientation of the purine and trimethoxyphenyl groups and the environment of the newly formed cavity can be used to understand the change in potency of most of the PU3 analogs synthesized to date.

There remains, however, one compound whose binding cannot be understood from this structural work. Chiosis et al. generated an R4-biotinylated PU3, which was demonstrated to bind to HSP90, TRAP1, and GRP94 [10]. In principle, such a major extension at the R4 position could be accommodated through the solvent-filled tunnel at the back of the trimethoxyphenyl cavity that reaches out into the solvent (with reference to Figure 1B, the tunnel is underneath the right-hand helix and on the face of the central β sheet). We have made series of compounds with extensions at R4 (data not shown): none show enzyme inhibition below 200 μM, and we have not been able to obtain a crystal structure for any of them.

Significance

The structures of the N-terminal domain of HSP90α and HSP90β are essentially identical and show remarkable plasticity in the loop region capping the ATP binding site. This is exploited by the PU3 series of compounds, which induce the formation of a distinctive pocket with the loop in a regular α helix. PU3-based inhibitors with enhanced potency have been

designed that elicit the expected molecular signature for cellular activity for inhibition of HSP90 activity. These structural studies provide a detailed rationale for most of the observed changes in affinity, highlighting the conformational changes and molecular interactions that can be exploited in the design of further improved HSP90 inhibitors for assessment as anticancer therapeutics.

Experimental Procedures

HSP90α
Protein Production
Both the hexa-histidine-tagged and untagged N-terminal fragment of HSP90α were overexpressed in the *E. coli* strain BL21 (P Lys S). The tag was added as an aid to purification, which, for the histidine-tagged protein, was carried out using a Ni affinity column followed by a monoQ ion-exchange column. Untagged protein was expressed in the same way as the tagged protein, but this protein lysate was run solely on the monoQ column. Both protein samples were concentrated to approximately 20 mg ml^{-1} using ultrafiltration into a final buffer containing 20 mM TRIS (pH 7.4) and 0.5 M NaCl. Accurate determination of protein concentration was achieved using a Bradford assay.

Crystallization
Initial conditions for crystallization of both hexa-histidine-tagged and untagged Nt-HSP90α protein were found using commercial screens. Screening was carried out using the 24-well hanging-drop vapor diffusion technique. Optimum conditions for both were found to be in solutions #3 and #6 of Clear Strategy Screen number 1 obtained from Molecular Dimensions. Both of these conditions contain 0.1 M Na Cacodylate (pH 6.5) and 25% PEG 2K MME. In addition, solution #3 contains 0.2 M MgCl$_2$ and solution #6 contains 0.8 M NaFormate. The reservoir well contained 500 μl of the precipitant solution, and the hanging drops were formed by mixing 2 μl of the proteins with 2 μl of the reservoir solution. The plates were left at +4°C. Crystals appeared within a few hours and were of a suitable size for data collection, in some cases, after overnight growth.

Structure Determination and Refinement
Crystals were transferred to cryoprotectant solution (crystallization reservoir solution with PEG concentration increased from 25% to 35%), and data were collected to 1.42 Å and 1.65 Å resolution for untagged and hexa-histidine-tagged Nt-HSP90α, respectively, at liquid N$_2$ temperature at the ESRF, stations ID14eh2 and ID14eh4. Diffraction data were processed using DENZO [20]. The N-terminal domain fragment of *apo* HSP90α (both his tagged and untagged) crystallizes in space group I222, with unit cell dimensions isomorphous to those of the previously solved HSP90α N-terminal domain fragment (PDB ID code 1YER). The structure was solved by isomorphous replacement using the 1YER model coordinates and the refinement program REFMAC5 [21]. Twenty cycles of rigid-body refinement followed by 20 cycles of restrained refinement were carried out. All model building was carried out using the molecular graphics program O [22], and refinement calculations were performed by REFMAC5. Following structure solution, difference electron density maps were calculated for the initial model and inspected. Crystallographic water molecules were added by cycling REFMAC with ARP [23]. Following each round of refinement, the models were adjusted and further solvent molecules were gradually added. The progress of the refinement was assessed using R$_{free}$ and the conventional R factor. Refinement converged at R$_{free}$/R factor values of 22.1%/18.3% and 22.7%/19.9% for the untagged and tagged protein. The final structures were validated using Procheck [24], and the untagged structure was deposited in the Protein Data Bank with ID code 1UYL. Full data collection and refinement statistics are presented in the Supplemental Data available with this article online.

HSP90α in Complex with PU3 Analogs
Crystallization
Crystals of the N-terminal HSP90α-PU3 complex were grown in the same conditions as the apo proteins, except 20 mM ligand solution was added to the protein solution, and the mixture was left to stand

on ice for 1 hr prior to setting up the crystallization trays. The compounds were synthesized as described in [12].

Structure Determination
The crystals were frozen in the same way as the apo crystals. Data were collected for Nt-HSP90α complexed to compound 1 on a Mar345 image plate on a Rigaku/MSC rotating anode at the University of York and processed using DENZO. Although the complex crystallized in the same space group as the apo protein, the unit cell parameters were nonisomorphous. The PU3-bound structure was solved by molecular replacement with AMoRe [25] using the apo HSP90α structure as the search model. All model building was carried out using the molecular graphics program O, and refinement calculations were performed with REFMAC5. Following structure solution, difference electron density maps were calculated for the initial model, the ligand structure was modeled into the difference density peaks, and the coordinates were refined before final addition of solvent. The progress of the refinement was assessed using R$_{free}$ and R factor, and the final structure was validated using PROCHECK and the CCP4 package [26].

Essentially identical crystallization, data collection, and refinement methods were used in the determination of the structure of Nt-HSP90α in complex with each of the compounds listed in Figure 4. All structures have been deposited in the Protein Data Bank with the codes shown in Figure 4, and the deposited files contain all data and refinement statistics. In summary, the resolution of data collected for the complexes ranged from 1.9 Å to 2.6 Å, and the structures were refined to R$_{free}$/R factor values of between 20.4%/17.2% and 21.4%/25.3%. Full data collection and refinement statistics are presented in the Supplemental Data.

HSP90β in Complex with PU3
Expression, Purification, and Crystallization
HSP90β 1-234 with a N-terminal 6×His tag was expressed in *E. coli* strain BL21-DE3. The protein was purified using a nickel-bound HiTrap column and then a ResourceQ column. The 6×His tag was removed by digestion with enterokinase, and the protein was repurified on the ResourceQ column. Nt-HSP90β complexed with PU3 was crystallized in 25% PEG MME 2000, 0.1 M Na Cacodylate (pH 6.5), 0.2 M MgCl$_2$.

Data Collection and Refinement
Crystals diffracted to 2.45 Å on an Raxis4 image plate mounted on a Rigaku MSC rotating anode source. The space group was the same as the Nt-HSP90α-PU3 crystal, I222, with cell dimensions of a = 66.8 Å, b = 90.6 Å, and c = 96.2 Å. A data set was collected from a single crystal, and the data were processed using Denzo and scaled with Scalepack. Molecular replacement using AMoRe within CCP4i used the native Nt-HSP90α structure as a model. Both rigid body and restrained refinement using REFMAC5 within CCP4i reduced the R factor and R$_{free}$. Maps showed that PU3 was bound and the conformation of the loop (residues 104–111) is the same as that of the Nt-HSP90α-PU3 structure. The residues that differ between the two structures were identifiable from the maps and rebuilt accordingly. The structure was refined to R$_{free}$/R factor values of 29.4%/23.5% and has been deposited in the PDB with ID code 1UYM. Full data collection and refinement statistics are presented in the Supplemental Data.

Assays
Malachite Green Assay for ATPase Activity
The malachite green assay for determining HSP90 ATPase activity has been described elsewhere [16]. Briefly, 0.42 mM yeast HSP90 is incubated overnight at 37°C in assay buffer (100 mM Tris-HCl [pH 7.4], 150 mM NaCl, 6 m MgCl$_2$) containing 370 μM ATP with or without test compound in DMSO (0.25%). The reaction is stopped by the addition of malachite green reagent (0.95% ammonium molybdate [from 5.725% stock in 6 M HCl], 0.027% malachite green, 0.3875% polyvinyl alcohol) followed by sodium citrate (2.96%). The absorbance is then determined at 620 nm.

Cell Lines
Human colon cell lines, HCT116, were obtained from ATCC (Manassas, USA). and were grown as monolayers in Dulbecco's modified Eagle's medium containing 10% fetal calf serum, 2 mM glutamine,

and nonessential amino acids in 6% CO_2/94% air. All lines were free of *Mycoplasma* contamination.

Growth Inhibition Studies

The sulfohodamine B assay (SRB) was used for growth inhibition studies as described previously [27]. Briefly, cells were seeded into 96-well microtiter plates and allowed to attach for 36 hr. Compounds at a range of concentrations were added in quadruplicate wells for 96 hr. Cells were then fixed with ice-cold 10% trichloroacetic acid and stained with 0.4% SRB in 1% acetic acid. The GI_{50} was calculated as the drug concentration that inhibits cell growth by 50% compared with control growth.

Western Blotting

Cells were treated with the compounds for 8, 16, 24, 48, 72, and 96 hr. The cells were then trypsinized, washed with PBS, lysed for 1 hr at 4°C in 100 μl lysis buffer (50 mM Tris-HCL, 150 mM NaCl [pH 7.5], 1% NP40, 2 mM PMSF, 10 μg/ml aprotenin, 10 μg/ml leupeptin, 1 mM $NaVO_4$, 1 mM NaF, 1 mM BGP), and protein concentration was determined. Lysates were centrifuged (MSE Microcentrifuge; 1200 rpm for 15 min at 4°C) and the resulting extracts were separated (70 μg/lane) by SDS-PAGE gel electrophoresis. The blots were probed for HSP70 (Stressgen, SPA 810), Raf-1 (Santa Cruz, SC133), CDK4 (Santa Cruz, SC260), ErbB2 (Santa Cruz, SC284), and GAPDH (Chemicon, MAB374). Antibody binding was identified with horse-radish peroxidase-labeled secondary antibodies combined with enhanced chemiluminescence reagents (Amersham) and autoradiography.

Molecular Modeling

All quantum-mechanical (QM) calculations were performed using the GAMESS program [28] at B3LYP/6-31G(d) level of theory. MIP values are calculated as the interaction between the molecule and a probe with the van der Waals parameters of a water molecule and a charge of +0.5 or −0.5 electron units. The electrostatic term is obtained by multiplying the QM-derived molecular electrostatic potential by the charge of the probe. The dispersion-repulsion term is accounted for by means of a pairwise-additive 6-12 Lennard-Jones potential using empirical parameters from the OPLS forcefield [29]. Van der Waals interaction energies between ligands and the protein were obtained using an in-house implementation of the Tripos van der Waals potential [18].

NMR Studies of Ligand Binding

Binding of N9-ethyl adenine and adenine to Nt-HSP90α was monitored by STD [30] and water-LOGSY [31] NMR experiments on a Bruker DRX 600 NMR spectrometer at 298 K. All NMR samples contained 50 mM potassium phosphate (pH 7.5), 10 μM Nt-HSP90α, 1 mM compound, and 10% D_2O. Competition was measured by direct addition of PU3 to the original NMR sample.

Supplemental Data

Supplemental Data consisting of a table of crystallographic data collection and refinement statistics for the 14 protein structures described in this article.are available at http://www.chembiol.com/cgi/content/full/11/6/775/DC1.

References

1. Maloney, A., and Workman, P. (2002). HSP90 as a new therapeutic target for cancer therapy: the story unfolds. Expert Opin. Biol. Ther. *2*, 3–24.

2. Isaacs, J.S., Xu, W., and Neckers, L. (2003). Heat shock protein 90 as a molecular target for cancer therapeutics. Cancer Cell *3*, 213–217.

3. Pearl, L.H., and Prodromou, C. (2001). Structure and in vivo function of HSP90. Curr. Opin. Struct. Biol. *10*, 46–51.

4. Marcu, M.G., Chadli, A., Bouhouche, I., Catelli, M., and Neckers, L.M. (2000). The heat shock protein 90 antagonist novobiocin interacts with a previously unrecognized ATP-binding domain in the carboxyl terminus of the chaperone. J. Biol. Chem. *275*, 37181–37186.

5. Langer, T., Schlatter, H., and Fasold, H. (2002). Evidence that the novobiocin-sensitive ATP-binding site of the heat shock protein 90 (HSP90) is necessary for its autophosphorylation. Cell Biol. Int. *26*, 653–657.

6. Meyer, P., Prodromou, C., Hu, B., Vaughan, C., Roe, S.M., Panaretou, B., Piper, P.W., and Pearl, L.H. (2003). Structural and functional analysis of the middle segment of hsp90: implications for ATP hydrolysis and client protein and cochaperone interactions. Mol. Cell *11*, 647–658.

7. Bergerat, A., de Massy, B., Gadelle, D., Varoutas, P.C., Nicolas, A., and Forterre, P. (1997). An atypical topoisomerase II from Archaea with implications for meiotic recombination. Nature *386*, 329–331.

8. Stebbins, C.E., Russo, A.A., Schneider, C., Rosen, N., Hartl, F.U., and Pavletich, N.P. (1997). Crystal structure of an HSP90-geldanamycin complex: targeting of a protein chaperone by an antitumor agent. Cell *89*, 239–250.

9. Dutta, R., and Inouye, M. (2000). GHKL, an emergent ATPase/kinase superfamily. Trends Biochem. Sci. *25*, 24–28.

10. Chiosis, G., Timaul, M.N., Lucas, B., Munster, P.N., Zheng, F.F., Sepp-Lorenzino, L., and Rosen, N. (2001). A small molecule designed to bind to the adenine nucleotide pocket of HSP90 causes Her2 degradation and the growth arrest and differentiation of breast cancer cells. Chem. Biol. *8*, 289–299.

11. Chiosis, G., Lucas, B., Shtil, A., Huezo, H., and Rosen, N. (2002). Development of a purine-scaffold novel class of HSP90 binders that inhibit the proliferation of cancer cells and induce the degradation of Her2 tyrosine kinase. Bioorg. Med. Chem. *10*, 55–64.

12. Dymock, B., Barril, X., Beswick, M., Collier, A., Davies, N., Drysdale, M., Fink, A., Fromont, C., Hubbard, R.E., Massey, A., et al. (2004). Adenine derived inhibitors of the molecular chaperone HSP90—SAR explained through multiple Xray structures. Bioorg. Med. Chem. Lett. *14*, 325–328.

13. Obermann, W.M., Sondermann, H., Russo, A.A., Pavletich, N.P., and Hartl, F.U. (1998). In vivo function of HSP90 is dependent on ATP binding and ATP hydrolysis. J. Cell Biol. *143*, 901–910.

14. Roe, S.M., Prodromou, C., O'Brian, R., Ladbury, J.E., Piper, P.W., and Pearl, L.H. (1999). Structural basis for inhibition of the HSP90 molecular chaperone by the antitumor antibiotics radicicol and geldanamycin. J. Med. Chem. *42*, 260–266.

15. Besant, P.G., Lasker, M.V., Bui, C.D., and Turck, C.W. (2002). Inhibition of branched-chain alpha-keto acid dehydrogenase kinase and Sln1 yeast histidine kinase by the antifungal antibiotic radicicol. Mol. Pharmacol. *62*, 289–296.

16. Rowlands, M.G., Newbatt, Y.M., Prodromou, C., Pearl, L.H., Workman, P., and Aherne, W. (2004). High throughput screening assay for inhibitors of heat-shock protein 90 (HSP90) ATPase activity. Anal. Biochem. *327*, 176–183.

17. Clarke, P.A., Hostein, I., Banerji, U., Stefano, F.D., Maloney, A., Walton, M., Judson, I., and Workman, P. (2000). Gene expression profiling of human colon cancer cells following inhibition of signal transduction by 17-allylamino-17-demethoxygeldanamycin, an inhibitor of the hsp90 molecular chaperone. Oncogene *19*, 4125–4133.

18. Clark, M., Cramer, R.D., III, and Van Opdenbosch, N. (1989). Validation of the general purpose tripos 5.2 force field. J. Comput. Chem. *10*, 982–1012.

19. Orozco, M., and Luque, F.J. (1993). Molecular interaction poten-

tial (MIP). A new tool for the theoretical study of molecular reactivity. J. Comput. Chem. *14*, 587–602.

20. Otwinowski, Z., and Minor, W. (1997). Processing of X-ray diffraction data collected in oscillation mode. In Methods in Enzymology, Volume 276, Macromolecular Crystallography, Part A, C.W. Carter, Jr. and R.M. Sweet, eds. (Academic Press), pp. 307–326.

21. Murshudov, G.N., Vagin, A.A., and Dodson, E.J. (1997). Refinement of macromolecular structures by the maximum-likelihood method. Acta Crystallogr. *D53*, 240–255.

22. Jones, T.A., Zou, J.Y., Cowan, S.W., and Kjeldgaard, M. (1991). Improved methods for building protein models in electron density maps and the location of errors in these models. Acta Crystallogr. *A47*, 110–119.

23. Lamzin, V.S., and Wilson, K.S. (1993). Automated refinement of protein models. Acta Crystallogr. *D49*, 129–149.

24. Laskowski, R.A., MacArthur, M.W., Moss, D.S., and Thornton, J.M. (1993). PROCHECK: a program to check the stereochemical quality of protein structures. J. Appl. Crystallogr. *26*, 283–291.

25. Navaza, J. (1994). AMoRe: an automated package for molecular replacement. Acta Crystallogr. *50*, 157–163.

26. CCP4 (Collaborative Computational Project, Number 4) (1994). The CCP4 suite: programs for protein crystallography. Acta Crystallogr. D Biol. Crystallogr. *50*, 760–763.

27. Skehan, P., Storeng, R., Scudiero, D., Monks, A., McMahon, J., Vistica, D., Warren, J.T., Bokesch, H., Kenney, S., et al. (1990). New colorimetric cytotoxicity assay for anticancer-drug screening. J. Natl. Cancer Inst. *82*, 1107–1112.

28. Schmidt, M.W., Baldridge, K.K., Boatz, J.A., Elbert, S.T., Gordon, M.S., Jensen, J.H., Koseki, S., Matsunaga, N., Nguyen, K.A., Su, S., et al. (1993). General atomic and molecular electronic structure system. J. Comput. Chem. *14*, 1347–1363.

29. Jorgensen, W.L., and Tirado-Rives, J. (1988). The OPLS (optimized potentials for liquid simulations) potential functions for proteins. Energy minimizations for crystals of cyclic peptides and crambin. J. Am. Chem. Soc. *110*, 1657–1666.

30. Mayer, M., and Meyer, B. (1999). Characterization of ligand binding by saturation transfer difference NMR spectroscopy. Angew. Chem. Int. Ed. Engl. *38*, 1784–1788.

31. Dalvit, C., Pevarello, P., Tato, M., Veronesi, M., Vulpetti, A., and Sundstrom, M. (2000). Identification of compounds with binding affinity to proteins via magnetization transfer from bulk water. J. Biomol. NMR *18*, 65–68.

32. Wallace, A.C., Laskowski, R.A., and Thornton, J.M. (1995). LIGPLOT: A program to generate schematic diagrams of protein-ligand interactions. Protein Eng. *8*, 127–134.

Accession Numbers

The structures of HSP90 described in this article have been deposited in the Protein Data Bank with the following ID codes: 1UYL, untagged HSP90α apo-structure; 1UYM, HSP90β complexed with PU3 (compound **1**); 1UY6, 1UY7, 1UY8, 1UY9, 1UYC, 1UYD, 1UYE, 1UYF, 1UYG, 1UYH, 1UYI, 1UYK, HSP90α complexed with compounds **1** to **12** of Figure 4, respectively.